Available on CMS information server **CMS NOTE 2006/036**

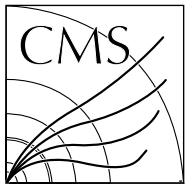

The Compact Muon Solenoid Experiment

CMS Note

Mailing address: CMS CERN, CH-1211 GENEVA 23, Switzerland

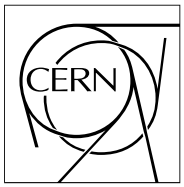

4 Feb. 2006

Measurement of Jets with the CMS Detector at the LHC

A. Heister [a)], O. Kodolova [b)], V. Konoplianikov [*) c)], S Petrushanko [b)], J. Rohlf [d)], C. Tully [e)], and A. Ulyanov [f)]

a) RWTH Aachen, Aachen, Germany
b) Moscow State University, Moscow, Russia
c) JINR, Dubna, Russia
d) Boston University, Boston, MA 02215, USA
e) Princeton University, Princeton, NJ 08544, USA
f) ITEP, Moscow, Russia

Abstract

The jet reconstruction algorithms and calibration techniques implemented in the CMS reconstruction software are studied with high-statistics Monte Carlo samples of QCD dijet events. Generated events are passed through a full detector-level simulation of the CMS detector including readout digitization in the presence of pile-up at an instantaneous luminosity of $\mathcal{L} = 2 \times 10^{33}\ \mathrm{cm}^{-2}\mathrm{s}^{-1}$. Effects of detector resolution and granularity on the jet resolutions, efficiencies and instrumental background rates are estimated. These measures of performance are compared for a set of jet algorithms, algorithm parameters, and calorimeter cell thresholds. The uniformity and linearity of the jet response are evaluated by comparing particle-level and reconstructed jets over a wide range of transverse momenta throughout the angular coverage of the calorimeters. Fits to the ratio of reconstructed to generated jet transverse energy give a transverse energy resolution of 10-15% (8-10%) at 100 GeV (200 GeV) over the pseudorapidity range $0 < |\eta| < 5$. The angular resolution for 100 GeV (200 GeV) jets is 0.02-0.035 (0.02) radians.

[*)] On leave from GSU, Gomel, Belarus

1 Introduction

Event signatures for SUSY, Higgs boson production, and other new physics processes require the reconstruction and measurement of jets coming from high-momentum quarks and gluons [1]. The problems with associating a jet measured in a calorimeter with a scattered parton is an old problem in hadron collisions [2]-[3]. The jet energy resolution and linearity are key factors in separating signal events from background and in measuring the properties of the signal. In this study, high statistics Monte Carlo samples of full detector-level simulated events are used to study jet reconstruction and performances with the CMS detector [4]. The simulation employs showering and energy loss processes for detailed modeling of particle interactions in the calorimeters [5]. Comparisons of the simulation with the measured single pion response from test beam data [6]-[8] are shown to reproduce the expected performance of the detector.

While the first jet algorithms for hadron colliders were simple cones [9], clusterng techniques have greatly improved in sophistication over the last two decades [10]-[11]. The approach taken in the performance evaluation of jets, as presented in this note, is to apply the jet finding and determine the corresponding jet responses for a set of jet reconstruction algorithms, parameters and calorimeter cell thresholds, chosen so as to achieve the highest efficiencies, resolutions and calibrated response linearies while maintaining a low instrumental fake rate. A "perfect-detector" jet is defined at particle-level through the use of jet algorithms, while a reconstructed jet is formed by applying the same algorithms on a set of energy deposits in calorimeter cells. A reconstructed jet is identified with the particle-level jet through a pseudorapidity, phi (η, ϕ) matching criterion that searches within a cone $R = \sqrt{\Delta\eta^2 + \Delta\phi^2}$ to find agreement of the jet axes. The correspondance of a reconstructed jet to the particle-level jet, however, is not always unambiguous. The parameters of the initial parton corresponding to the particle jet depends on a number of factors including final state radiation, which can lead to the splitting of the jet in the detector. For a large cone, the jet reconstruction collects a large fraction of the energy of the initial parton, but such a cone is also susceptible to collecting the energy of non-isolated additional partons in the hard interaction, in addition to energy from the underlying event, pile-up interactions, and electronic noise. For example, with a tower transverse energy threshold cut of $E_{\rm T} = 0.5$ GeV, an estimated 5 GeV of electronic noise is collected in a cone of $R = 0.5$ and the event pile-up at low luminosity pile-up ($\mathcal{L} = 2 \times 10^{33}$ cm^{-2}s^{-1}) will contribute approximately 2.5 GeV.

The first step in the reconstruction, before invoking the jet algorithm, is to apply noise and pile-up suppression with either a set of cuts on the tower energies or to apply a pile-up subtraction algorithm [12]. The choice of the tower energy or $E_{\rm T}$ cuts is based on a balance between jet reconstruction efficiency and instrumental fake rates. The factors influencing the identification of a reconstructed jet energy with the energy of a scattered parton can be divided into two groups. One is connected with the jet as a physical object, and includes fragmentation model, initial and final state radiation, the underlying event, and particles coming from pile-up events. A second group follows from detector performance and includes electronic noise, the effect of the magnetic field which deflects low energy charged particles out of the jet reconstruction cone, non-compesating responses of the calorimeters to electromagnetic and hadronic showers (electron/hadron ratio), losses due to out-of-cone showering, dead materials and cracks and longitudinal leakage for high energy jets. While some of the corrections for effects in the first group are channel dependent, the bulk of the detector effects are channel independent and common particle-level correction coefficients can be provided.

Calibrations are applied to restore equality between reconstructed and particle-level jets. Corrections to the jet energy have a strong dependence on η and $E_{\rm T}$. These non-uniformities are due in part from differing detector technologies versus η, granularity changes in η and ϕ, subdetector boundaries, and the intrinsic E-dependence (as opposed to $E_{\rm T}$) in the detector response. The impact of these non-uniformities and the complication of additional pile-up energy in the forward detectors is also reflected in the η dependence of the instrumental background rates for misreconstructed jets.

2 Jet Algorithms and Recombination Schemes

There are three principal jet reconstruction algorithms included in this study: the iterative cone [13, 14], the midpoint cone [10, 15] and the inclusive $k_{\rm T}$ jet algorithm [11, 16, 17] The midpoint-cone and $k_{\rm T}$ algorithms are widely used in offline analysis in current hadron collider experiments [18] while the iterative cone algorithm is simpler and faster and commonly used for jet reconstruction in software-based trigger systems.

The jet algorithms may be used with one of two recombination schemes for adding the constituents. In the energy scheme, constituents are simply added as four vectors. This produces massive jets. In the $E_{\rm T}$ scheme, massless jets are produced by equating the jet transverse momentum to the $\Sigma E_{\rm T}$ of the constituents and then fixing the direction

of the jet in one of two ways: 1) $\sin\theta = \Sigma E_{\rm T}/E$ where E is the jet energy (usually used with cone algorithms), or 2) $\eta = \Sigma E_{{\rm T}i}\eta_i/\Sigma E_{\rm T}$ and $\varphi = \Sigma E_{{\rm T}i}\varphi_i/\Sigma E_{\rm T}$ (usually used with the $k_{\rm T}$ algorithm). When using the $E_{\rm T}$ scheme, the jet $E_{\rm T}$ is equal to $p_{\rm T}c$.

The inclusive $k_{\rm T}$ algorithm merges, in each iteration step, input objects into possible final jets and so the new jet quantities, the jet direction and energy, have to be calculated directly during the clustering. The cone jet algorithms, iterative and midpoint, group the input objects together as an intermediate stage and the final determination of the jet quantities (recombination) is done in one step at the end of the jet finding.

2.1 Iterative Cone

In the iterative cone algorithm, an $E_{\rm T}$-ordered list of input objects (particles or calorimeter towers) is created. A cone of size R in η,φ space is cast around the input object having the largest transverse energy above a specified seed threshold. The objects inside the cone are used to calculate a *proto-jet* direction and energy using the $E_{\rm T}$ scheme. The computed direction is used to seed a new proto-jet. The procedure is repeated until the energy of the proto-jet changes by less than 1% between iterations and the direction of the proto-jet changes by $\Delta R < 0.01$. When a stable proto-jet is found, all objects in the proto-jet are removed from the list of input objects and the stable proto-jet is added to the list of jets. The whole procedure is repeated until the list contains no more objects with an $E_{\rm T}$ above the seed threshold. The cone size and the seed threshold are parameters of the algorithm. When the algorithm is terminated, a different recombination scheme may be applied to jet constituents to define the final jet kinematic properties.

2.2 Midpoint Cone

The midpont-cone algorithm was designed to facilitate the splitting and merging of jets. The midpoint-cone algorithm also uses an iterative procedure to find stable cones (proto-jets) starting from the cones around objects with an $E_{\rm T}$ above a seed threshold. Contrary to the iterative cone algorithm described above, no object is removed from the input list. This can result in overlapping proto-jets (a single input object may belong to several proto-jets). To ensure the collinear and infrared safety of the algorithm, a second iteration of the list of stable jets is done. For every pair of proto-jets that are closer than the cone diameter, a *midpoint* is calculated as the direction of the combined momentum. These midpoints are then used as additional seeds to find more proto-jets. When all proto-jets are found, the splitting and merging procedure is applied, starting with the highest $E_{\rm T}$ proto-jet. If the proto-jet does not share objects with other proto-jets, it is defined as a jet and removed from the proto-jet list. Otherwise, the transverse energy shared with the highest $E_{\rm T}$ neighbor proto-jet is compared to the total transverse energy of this neighbor proto-jet. If the fraction is greater than f (typically 50%) the proto-jets are merged, otherwise the shared objects are individually assigned to the proto-jet that is closest in η,φ space. The procedure is repeated, again always starting with the highest $E_{\rm T}$ proto-jet, until no proto-jets are left. This algorithm implements the energy scheme to calculate the proto-jet properties but a different recombination scheme may be used for the final jet. The parameters of the algorithm include a seed threshold, a cone radius, a threshold f on the shared energy fraction for jet merging, and also a maximum number of proto-jets that are used to calculate midpoints.

2.3 Inclusive $k_{\rm T}$kT Algorithm

The inclusive $k_{\rm T}$ jet algorithm is a cluster-based jet algorithm. The cluster procedure starts with a list of input objects, stable particles or calorimeter cells. For each object i and each pair (i,j) the following distances are calculated:

$$\begin{aligned} d_i &= (E_{{\rm T},i})^2 R^2, \\ d_{ij} &= min\{E^2_{{\rm T},i}\,,\, E^2_{{\rm T},j}\} R^2_{ij} \quad \text{with} \quad R^2_{ij} = (\eta_i - \eta_j)^2 + (\varphi_i - \varphi_j)^2, \end{aligned}$$

where R^2 is a dimensionless parameter normally set to unity [10]. The algorithm searches for the smallest d_i or d_{ij}. If a value of type d_{ij} is the smallest, the corresponding objects i and j are removed from the list of input objects. They are merged using one of the recombination schemes listed below and filled as one new object into the list of input objects. If a distance of type d_i is the smallest, then the corresponding object i is removed from the list of input objects and filled into the list of final jets. The procedure is repeated until all objects are included in jets. The algorithm successively merges objects which have a distance $R_{ij} < R$. It follows that $R_{ij} > R$ for all final jets i and j.

3 Efficiencies and Instrumental Background Rates

Jet reconstruction algorithms are applied to projective calorimeter towers with a granularity set by the η, ϕ dimensions of the hadronic calorimeter cells [8]. The electromagnetic calorimeter covers the barrel and encdap region with a 5 times smaller cell size. In the central η region, corresponding to $|\eta| < 1.305$, a "tail-catcher" outer hadronic calorimeter is present. The transition region between the barrel and endcaps is in the $1.305 < |\eta| < 1.479$ range. The η, ϕ granularity of the hadronic calorimeter is a constant $0.087, 0.087$ for $|\eta| < 1.74$ corresponding to tower η-indices 1-20. Beyond $|\eta| = 1.74$, the endcap increases in ϕ-granularity from 0.087 cells to 0.175 cells in the $1.74 < |\eta| < 3.00$ range corresponding to tower η-indices 21-28 [1)]. In the overlapping η range of $2.853 < |\eta| < 5.191$ is the forward hadronic calorimeter with a nearly constant η, ϕ granularity of $0.175, 0.0175$ over the $2.964 < |\eta| < 4.716$ range corresponding to η indices 29-41.

These geometrical transitions affect the uniformity of the jet reconstruction in terms of efficiencies and instrumental background rates. There is a balance to be struck between jet reconstruction efficiency at low energy and the instrumental background rates. A large part of the efficiency/background trade-off comes from the choice of calorimeter cell thresholds. This study includes five threshold schemes: 1) $E_{\mathrm{T}} > 0$ GeV, 2) $E_{\mathrm{T}} > 0.5$ GeV, 3) $E_{\mathrm{T}} > 0.5$ GeV and $E > 0.8$ GeV, 4) $E_{\mathrm{T}} > 1.0$ GeV, and 5) underlying event (UEInput) scheme. The UEInput scheme is a data-driven technique for estimating the average energy in a tower as a function of the η index. This method computes the average energy in a tower for towers outside of the reconstructed jets in the event and these energies are used to set η-dependent cell thresholds. The thresholds used in this study are presented in Table 1. The UEInput is intended to be data-driven and the thresholds depend on the instantaneous luminosity, although there is some underlying event contribution, especially at low luminosity, and therefore some process dependence. The same thresholds are applied when deriving jet calibrations, for example from gamma+jet or dijet balancing, so although the thresholds are optimized to suppress unclustered η-dependent contributions to the jet reconstruction from particular data triggers, the reconstructed jets will have the proper average particle-level calibrations. The $\mathrm{t\bar{t}H}$ sample was chosen because it is an example of a multijet environment where jet fake rate reduction is quite relevant. It does give good threshold settings with low fake rate implying that if we have a greatly differing underlying event for a particular process, the data may be used to adapt the thresholds for the jet algorithms.

Table 1: The energy thresholds corresponding to a data-driven measure of the η-dependent energy flow from Monte Carlo simulated underlying events from $\mathrm{t\bar{t}H}$ production ("UEInput-scheme"). The energy thresholds corresponding to the calorimeter tower η indices are given along with the value of the maximum $|\eta|$ boundary of the tower(s).

η index	1-16	17	18	19	20	21	22	23	24	25	26
$\|\eta\|$ maximum	1.392	1.479	1.566	1.653	1.740	1.830	1.930	2.043	2.172	2.322	2.500
E threshold (GeV)	1.50	1.60	1.77	1.97	2.21	2.49	2.83	3.28	3.86	4.65	5.73
η index	27	28-29	30	31	32	33	34-41				
$\|\eta\|$ maximum	2.650	3.000	3.139	3.314	3.489	3.664	5.191				
E threshold (GeV)	6.98	9.20	11.50	13.41	15.38	17.36	1.69+4.6·$\|\eta\|$				

The event samples used for the analysis are dijet events simulated for $\hat{p}_{\mathrm{T}}$ bins 0-15, 15-20, 20-30, 30-50, 50-80, and 80-120 GeV/c. There is a strong dependence in the jet response linearity at low E_{T} on the calorimeter threshold settings. Therefore, to compare jet performances for different tower thresholds, it is necessary to set a common operating point for the jet efficiency, defined to be the percentage of all particle-level jets, for a particular bin in E_{T}, that match with a reconstructed jet within a cone of $R = 0.3$. This is done by requiring the jet efficiency for a 20 GeV particle-level jet, $E_{\mathrm{T}}^{\mathrm{MC}} = 20$ GeV, to be equal to 50%. This point was chosen to accomodate a minimum uncalibrated jet reconstruction threshold of $E_{\mathrm{T}}^{\mathrm{Rec}} = 3$ GeV for the range of studied threshold settings. The threshold settings and their corresponding $E_{\mathrm{T}}^{\mathrm{Rec}}$ thresholds required to give exactly 50% jet finding efficiency at $E_{\mathrm{T}}^{\mathrm{MC}} = 20$ GeV for $\eta < 2.5$ are listed in Table 2 for the iterative cone algorithm with cone radius $R = 0.5$ using the E scheme.

The corresponding jet efficiency curves *vs.* generated jet E_{T} for the five different threshold schemes are shown in Fig. 1. They are remarkably similar in shape indicating that the corresponding jet resolutions for the different threshold schemes are very similar. The instrumental background rate is defined in this study to be the number of reconstructed jets per event that have no match with particle-level jets with $E_{\mathrm{T}}^{\mathrm{MC}} > 10$ GeV within a cone radius

[1)] Tower 28 will be split in the final readout geometry into two η-regions divided at $\eta = 2.868$ in the first two longitudinal segmentations [8].

Table 2: The threshold settings and their corresponding $E_{\mathrm{T}}^{\mathrm{Rec}}$ thresholds required to give exactly 50% jet finding efficiency at $E_{\mathrm{T}}^{\mathrm{MC}} = 20$ GeV for $\eta < 2.5$ for the iterative cone algorithm with cone radius $R = 0.5$ using the E scheme. The matching criterion for this study is $\Delta R < 0.3$. The fake rates are calculated from dijets event samples with 50 GeV $< \hat{p}_{\mathrm{T}} <$ 80 GeV.

Tower threshold (GeV)	$E_{\mathrm{T}} > 0$	$E_{\mathrm{T}} > 0.5$	$E_{\mathrm{T}} > 0.5$, $E > 0.8$	$E_{\mathrm{T}} > 1.0$	UEInput
Reconstructed jet E_{T} threshold (GeV)	15	10.1	8.46	5.86	5.6
Fake rate for $\eta < 2.5$ (jets/event)	1.343	1.360	0.678	0.773	0.815
Fake rate for the full η range (jets/event)	2.00	1.98	1.64	2.10	2.29

of $R = 0.3$ for jets above the $E_{\mathrm{T}}^{\mathrm{Rec}}$ threshold corresponding to a common efficiency point described above. The particles from pile-up events are not included in the list of particle-level jets and therefore in this definition, pile-up jets will contribute to the jet fake rate. The fake rates for different tower thresholds are reported in Table 2.

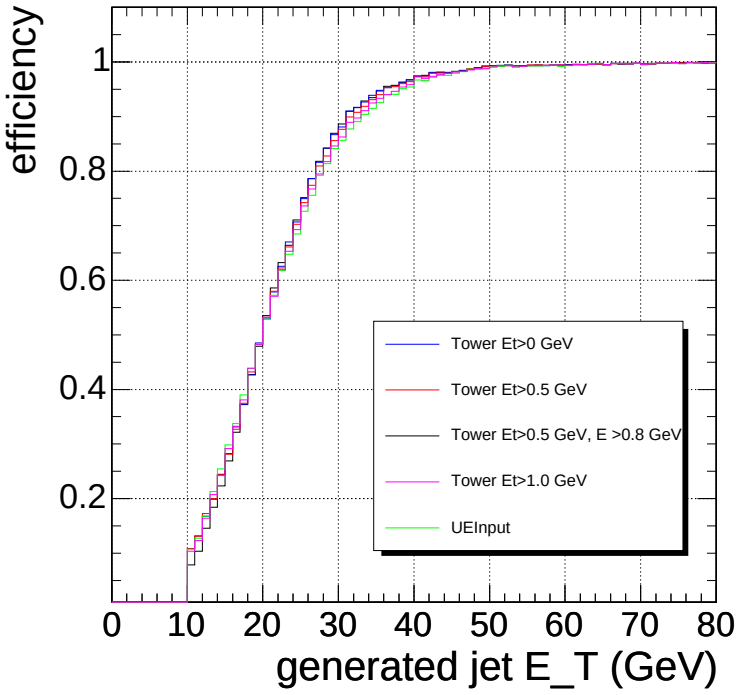

Figure 1: Jet efficiency curves for five different threshold schemes.

4 Monte Carlo Calibration of Jet Response

Jet response was studied with QCD dijet samples in $\hat{p}_{\mathrm{T}}$-bins over the range 0-4500 GeV. These Monte Carlo samples were generated with PYTHIA 6.214 [19], simulated in the CMS detector by OSCAR 245 [20] and digitized by ORCA 761 [21]. The statistics used in this study consists of 220k low-luminosity events (22 different QCD $\hat{p}_{\mathrm{T}}$ bins, 10k events each) [22].

The jets were reconstructed using the iterative cone algorithm (R = 0.5), midpoint cone, and cluster-based k_{T} technique using the E_{T} scheme. Particle-level and reconstructed jets were found by applying the same jet algorithm to stable particles (excluding neutrinos and muons) and calorimeter cells, respectively. A matching criterion, based on the distance $\Delta R = \sqrt{\Delta\eta^2 + \Delta\phi^2} < 0.2$, was used to associate particle-level and reconstructed jets. ORCA 873 was used to reconstruct and retrieve the jet information from the events.

The range of pseudo-rapidity $|\eta| < 4.8$ was divided into 16 regions. For each region the ratio of reconstructed jet transverse energy to the particle-level jet transverse energy, $R_{\mathrm{jet}} = E_{\mathrm{T}}^{\mathrm{Rec}}/E_{\mathrm{T}}^{\mathrm{MC}}$, as a function of $E_{\mathrm{T}}^{\mathrm{MC}}$ was approximated by the set of functions:

1. For $E_{\rm T}^{\rm MC} < E_1$: $R_{\rm jet} = a_1\sqrt{E_{\rm T}^{\rm MC} + a_2} + a_3$;

2. For $E_{\rm T}^{\rm MC} > E_2$: $R_{\rm jet} = a_4/\sqrt{a_5 E_{\rm T}^{\rm MC} + a_6} + a_7$;

3. For $E_1 < E_{\rm T}^{\rm MC} < E_2$: this part was approximated by a linear function $R_{\rm jet} = b_1 E_{\rm T}^{\rm MC} + b_2$, which goes through the points ($E_{\rm T}^{\rm MC} = E_1, a_1\sqrt{E_1 + a_2}+a_3$) and ($E_{\rm T}^{\rm MC} = E_2, a_4/\sqrt{a_5 E_2 + a_6}+a_7$) thereby defining the parameters b_1 and b_2.

The $R_{\rm jet}$ dependence as a function of $E_{\rm T}^{\rm MC}$ was used to determine the calibration coefficient K. In order to reduce the resolution effects from the $p_{\rm T}$-dependence of the calibration sample, an iterative procedure is applied. Initially we set the correction coefficients equal to unity, namely $E_{\rm T}^{\rm Corr} = E_{\rm T}^{\rm Rec}$, and compute the average response under this assumption to determine $K_1 = R_{\rm jet}$, using MC information from the particle-jet $E_{\rm T}^{\rm MC}$. For reconstructed jets with $E_{\rm T}^{\rm Rec} < 10$ GeV we compute the response assuming $E_{\rm T}^{\rm Corr} = 10$ GeV. In the second iteration, we set $E_{\rm T}^{\rm Corr} = E_{\rm T}^{\rm Rec}/K_1$ and compute $K_2 = R_{\rm jet}$. After 10 iterations the calibration coefficient $K = K_{10}$ has converged and is used to correct the jet transverse energy measurement: $E_{\rm T}^{\rm Corr} = E_{\rm T}^{\rm Rec}/K$.

Figs. 2 shows the ratio $R_{\rm jet}$ as a function of η for different generated jet transverse energies before the MC jet correction, using the iterative cone algorithm, similar results were obtained with the $k_{\rm T}$-jets and midoint cone algorithms.

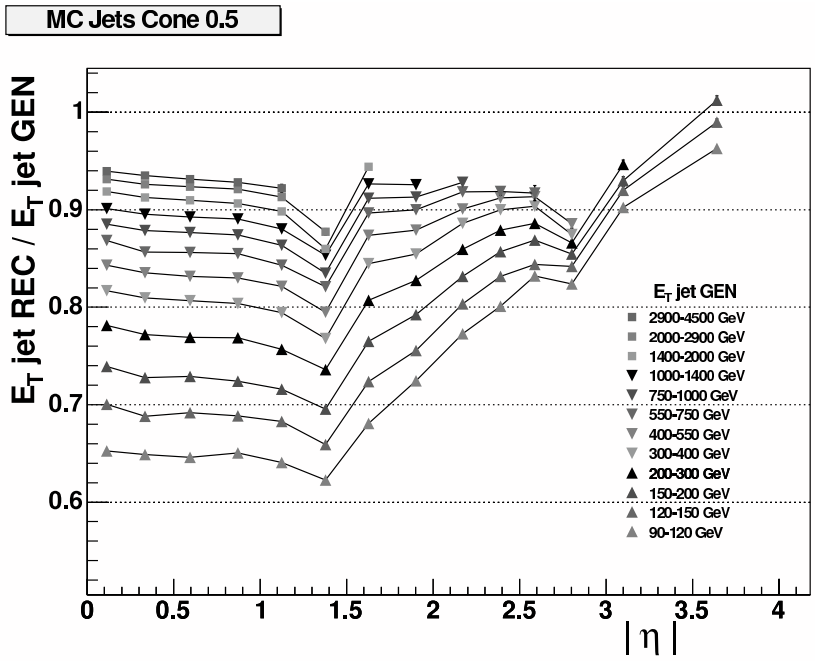

Figure 2: The ratio of the reconstructed jet transverse energy $E_{\rm T}^{\rm Rec}$ to the generated transverse energy $E_{\rm T}^{\rm MC}$ as a function of pseudorapidity of generated jet $|\eta|$ for jets with different $E_{\rm T}^{\rm MC}$ reconstructed by the interative cone $R = 0.5$ algorithm before MC jet calibration.

A summary of the fitted coeficients, $a_1 - a_7$ and $E_1 - E_2$, is given in Tables 3 and 4.

Taking independent statistical samples of QCD dijet events and fitting the linearity and offset of the corrected spectrum of transverse energies shows that the MC jet calibration method achieves an accuracy of 0.7 GeV on the offset and 0.3% on the slope of $E_{\rm T}^{\rm Corr}$ versus $E_{\rm T}^{\rm MC}$. This is estimated using the maximum deviations of the fits from 4 η ranges from barrel to very forward η regions. The calibration of the absolute jet energy scale will be determined from the data in processes such as γ+jet, Z+jet and $\rm t\bar{t}(W \rightarrow jets)$ which leverage on the knowledge of know particle resonances or the high resolution of the electromagnetic calorimeter.

5 Jet Resolution

The jet resolution was determined from a sample of QCD dijet events generated with PYTHIA 6.226. The events were fully simulated with OSCAR 365, and digitized and reconstructed wiht pileup accrding to a luminosity of

Table 3: The coefficients $a_1 - a_7$ and $E_1 - E_2$ for the MC jet calibration for iterative cone algorithm (with cone size $R = 0.5$).

η	E_1	E_2	a_1	a_2	a_3	a_4	a_5	a_6	a_7
0–0.226	70.0	90.0	0.33689	1697.88	-13.5896	-1.00239	0.10000	-1.50000	0.99493
0.226–0.441	70.0	90.0	0.45156	3366.14	-25.9109	-1.08241	0.10000	-1.05000	0.99496
0.441–0.751	70.0	90.0	0.09177	74.6907	-0.53484	-1.07299	0.10000	-0.95000	0.99199
0.751–0.991	70.0	90.0	0.38624	3005.81	-20.8524	-1.91313	0.31209	-0.80000	0.99036
0.991–1.260	70.0	90.0	0.27034	1344.17	-9.59419	-2.98238	0.62589	8.71840	0.99025
1.260-1.496	80.0	120.0	0.06937	95.6110	-0.34605	-2.73402	0.96289	-19.1834	0.93249
1.496–1.757	60.0	80.0	0.35583	1766.24	-14.6365	-4.64909	2.53255	-49.3323	1.01356
1.757–2.046	60.0	80.0	0.43001	2034.94	-19.0616	-3.91652	2.28764	-35.0517	1.00364
2.046–2.295	60.0	80.0	0.08378	20.6507	-0.06227	-3.28742	2.12328	-22.5683	1.00901
2.295–2.487	50.0	60.0	0.07300	3.55373	0.17113	-2.32246	1.80381	-23.4979	0.98817
2.487–2.690	45.0	55.0	0.05332	-5.32874	0.40227	-1.43751	1.20285	-16.0724	0.97114
2.690–2.916	35.0	45.0	0.05409	3.22465	0.39711	-1.85939	2.21389	-1.00000	0.94701
2.916–3.284	35.0	45.0	0.04791	-5.87386	0.53758	-0.67138	0.26078	-1.22056	1.03377
3.284–4.000	35.0	45.0	0.05059	-9.03556	0.61924	-1.15244	1.32254	-18.5026	1.07971
4.000–4.400	15.0	16.0	0.09776	-0.01017	0.35675	-1.65606	1.28359	-1.78008	1.12658
4.400–4.800	15.0	16.0	0.08225	-0.00882	0.30002	-34.6967	614.711	-1.00002	0.97188

Table 4: The coefficients $a_1 - a_7$ and $E_1 - E_2$ for the MC jet calibration for the cluster-based k_{T} algorithm (with the E_{T}-scheme).

η	E_1	E_2	a_1	a_2	a_3	a_4	a_5	a_6	a_7
0.226	35.0	45.0	0.21187	2530.94	-10.4062	-3.03685	0.46279	2.15441	1.01592
0.441	50.0	65.0	0.50248	2446.67	-24.7056	-1.27760	0.10000	-1.00000	1.00081
0.751	70.0	90.0	0.35719	2087.85	-16.0951	-1.29309	0.10000	-0.95000	1.00016
0.991	70.0	90.0	0.05185	0.04622	0.07389	-1.77282	0.19052	-0.80000	0.99772
1.260	70.0	90.0	0.34232	2080.02	-15.3620	-3.15359	0.51638	6.44417	0.99904
1.496	90.0	120.0	0.07139	73.4669	-0.35420	-3.45394	0.68219	5.73943	0.97998
1.757	60.0	80.0	0.09021	39.7461	-0.38418	-27.6310	43.4308	-1.00000	1.05097
2.046	60.0	80.0	0.42640	1743.57	-17.5434	-6.90712	3.64679	-4.81334	1.03843
2.295	60.0	80.0	0.06557	-4.39938	0.13709	-3.92938	2.16084	-33.9830	1.02645
2.487	50.0	60.0	0.43229	1288.20	-15.1789	-3.16147	2.05124	-35.1051	1.01577
2.690	45.0	55.0	0.53879	1963.09	-23.4812	-2.19956	1.35390	-14.4182	0.99705
2.916	35.0	45.0	0.44573	1814.56	-18.5445	-2.70847	2.51746	-32.6891	0.98825
3.284	35.0	45.0	0.42950	1439.95	-15.8126	-1.86773	1.03944	-12.9134	1.06381
4.000	25.0	30.0	0.42679	648.381	-10.4089	-1.95243	1.07706	-11.6884	1.13723
4.400	26.0	27.0	0.07047	-3.15964	0.33342	-3.90660	4.58056	-49.8324	1.13114
4.800	25.0	26.0	0.04358	-6.74910	0.36922	-1.41126	2.76134	-48.0064	0.85629

($\mathcal{L} = 2 \times 10^{33}\mathrm{cm}^{-2}\mathrm{s}^{-1}$). The sample was split into 21 bins of $\hat{\mathrm{p}}_\mathrm{T}$ with a statistics of 10k events per $\hat{\mathrm{p}}_\mathrm{T}$ bin. All jets reconstructed in these events are included in the resolution fits. For the purpose of evaluating the linearity of the jet response, particle-level jets were reconstructed from all stable particles (excluding neutrinos and muons) using two different jet algorithms: the iterative cone algorithm with a cone size $R = 0.5$ and the cluster-based k_T algorithm. The E_T recombination scheme was used in both jet algorithms. The particle-level jets are required to have $|\eta| < 5$, corresponding to the full η coverage of the calorimeters. A matching criteria based on the distance $R = \sqrt{(\phi^2 + d\eta^2)}$ is used to associate particle-level and reconstructed jets axes. Two different matching criteria $R = 0.1$ (for comparison with ref. [23]) and $R = 0.2$ were used for this study. Examples of fits are shown in Figs. 3-4.

The resolution plots were fitted with the following functional form:

$$\frac{\sigma(\frac{E_\mathrm{T}^\mathrm{Rec}}{E_\mathrm{T}^\mathrm{MC}})}{< \frac{E_\mathrm{T}^\mathrm{Rec}}{E_\mathrm{T}^\mathrm{MC}} >} = \frac{a}{E_\mathrm{T}^\mathrm{MC}} \oplus \frac{b}{\sqrt{E_\mathrm{T}^\mathrm{MC}}} \oplus c \tag{1}$$

where the first term is due to fixed energy fluctuations in the cone from electronics noise, pile-up and underlying event energy, the second term comes from the stocastic response of the calorimeter measurements and the last term is the constant term from residual non-uniformities and non-linearities in the detector response. The fits were done down to a transverse energies of 30 GeV in the barrel and endcap and 20 GeV in the forward region.

The jet resolution, calibrated with the Monte Carlo jet correction function, is shown in Fig. 5. The resolution curves for the barrel, endcap and forward regions are shown in Fig. 6 for the iterative cone $R = 0.5$ algorithm with the Monte Carlo jet calibration applied. The result of the fits are presented in Table 5. The Monte Carlo jet calibration improves the resolution in barrel region.

Table 5: Jet energy resolution parameters in 3 η regions of the calorimeters for the iterative cone $R = 0.5$ and k_T algorithms with the E_T recombination scheme.

	$\lvert\eta\rvert < 1.4$ (EB+HB+HO)	$1.4 < \lvert\eta\rvert < 3.0$ (EE+HE)	$3.0 < \lvert\eta\rvert < 5.0$ (HF)
IC, $\Delta R < 0.1$, raw	$\frac{6.6}{E_\mathrm{T}^{MC}} \oplus \frac{1.39}{\sqrt{E_\mathrm{T}^{MC}}} \oplus 0.036$	$\frac{7.9}{E_\mathrm{T}^{MC}} \oplus \frac{0.70}{\sqrt{E_\mathrm{T}^{MC}}} \oplus 0.048$	$\frac{3.24}{E_\mathrm{T}^{MC}} \oplus \frac{0.48}{\sqrt{E_\mathrm{T}^{MC}}} \oplus 0.077$
IC, $\Delta R < 0.2$, raw	$\frac{7.5}{E_\mathrm{T}^{MC}} \oplus \frac{1.44}{\sqrt{E_\mathrm{T}^{MC}}} \oplus 0.034$	$\frac{8.5}{E_\mathrm{T}^{MC}} \oplus \frac{0.67}{\sqrt{E_\mathrm{T}^{MC}}} \oplus 0.049$	$\frac{4.1}{E_\mathrm{T}^{MC}} \oplus \frac{0.2}{\sqrt{E_\mathrm{T}^{MC}}} \oplus 0.087$
IC, $\Delta R < 0.2$, calib	$\frac{5.6}{E_\mathrm{T}^{MC}} \oplus \frac{1.25}{\sqrt{E_\mathrm{T}^{MC}}} \oplus 0.033$	$\frac{4.8}{E_\mathrm{T}^{MC}} \oplus \frac{0.89}{\sqrt{E_\mathrm{T}^{MC}}} \oplus 0.043$	$\frac{3.8}{E_\mathrm{T}^{MC}} \oplus 0.085$
k_T, $\Delta R < 0.2$, raw	$\frac{10.6}{E_\mathrm{T}^{MC}} \oplus \frac{1.57}{\sqrt{E_\mathrm{T}^{MC}}} \oplus 0.027$	$\frac{13.5}{E_\mathrm{T}^{MC}} \oplus \frac{1.06}{\sqrt{E_\mathrm{T}^{MC}}} \oplus 0.038$	$\frac{6.5}{E_\mathrm{T}^{MC}} \oplus 0.089$

The resolution curves on the measurement of ϕ and η of the jets for the barrel, endcap and very forward regions are shown in Figs. 7 and 8 for the iterative cone algorithm, $R = 0.5$.

Finally, we note that the calibration coefficients are model dependent in the sense that any changes in our theoretical understanding of QCD processes (for example, taking into account high-order corrections) can shift the coefficients such that the Monte Carlo calibration procedure must be repeated.

6 Summary

The jet reconstruction algorithms and Monte Carlo calibration techniques have been studied with CMS full detector-level simulation of QCD dijet events in the presence of pile-up at an instantaneous luminosity of $\mathcal{L} = 2 \times 10^{33}\ \mathrm{cm}^{-2}\mathrm{s}^{-1}$. The uniformity and linearity of the jet response have been evaluated by comparing particle-level and reconstructed jets over a wide range of transverse momenta throughout the angular coverage of the calorimeters.

References

[1] See, for example, E. Eichten, I. Hinchliffe, K. Lane, and C. Quigg, "Supercollider Physics", *Rev. Mod. Phys.* **56** (1984) 579; J. Branson *et al.*, "High Transverse Momentum Physics at the Large Hadron Collider,"

EPJdirect **CN1** (2002) 1; M. Carena and H. E. Haber, "Higgs Boson Theory and Phenomenology," hep-ph/0208209, *Prog. Part. Nucl. Phys.* **50** (2003) 63; J. Rohlf, "Physics with Jets at the LHC," Acta Phys. Polon. **B36** 469 (2005).

[2] C. Bromberg *et al.*, "Observation of the Production of Jets of Particles at High Transverse Momentum and Comparison with Inclusive Single Particle Reactions," Phys. Rev. Lett. **38**, 1447 (1977); C. Bromberg *et al.*, "Experimental Tests of Quantum Chromodynamics in High p_{T} Jet Production in 200-GeV/c Hadron-Proton Collisions," Phys. Rev. Lett. **43**, 565 (1979); J. Rohlf, PhD Thesis, Caltech, "Jet Production in High-Energy Hadron-Proton Collisions," published in *Nucl. Phys.* **B171** (1980) 1.

[3] G. Arnison *et al.*, "Angular Distributions and Structure Functions from Two-Jet Events at the CERN SPS $\mathrm{p\bar{p}}$ Collider," *Phys. Lett.* **B136** (1984) 294; G. Arnison *et al.*, "Angular Distributions for High-Mass Jet Pairs and a Limit of the Energy Scale for Compositeness for Quarks from the CERN $\mathrm{p\bar{p}}$ Collider," *Phys. Lett.* **177B** (1986) 244.

[4] The Compact Muon Solenoid, Letter of Intent, CERN/LHCC 92-3, LHCC/I 1, (1992).

[5] CMS, The Hadron Calorimeter Project: Technical Design Report, CERN/LHCC 97-32 (1997); CMS, The Electromagnetic Calorimeter Project: Technical Design Report, CERN/LHCC 97-33 (1997).

[6] V. V. Abramov *et al.* [CMS-HCAL Collaboration], "Studies of the Response of the Prototype CMS Hadron Calorimeter, Including Magnetic Field Effects, to Pion, Electron, and Muon Beams," Nucl. Instr. and Meth. A 457 (2001) 75.

[7] V. D. Elvira, "Validation of Geant4 Physics Using the CMS HCAL Test Beam 2002 Experiment," CMS Note 2004/021 (2004).

[8] CMS HCAL Collaboration, "Design, Performance, and Calibration of CMS Hadron-Barrel Calorimeter Wedges," "Design, Performance, and Calibration of CMS Hadron-Endcap Calorimeter Wedges," "Design, Performance, and Calibration of CMS Forward Calorimeter Wedges," "Longitudinal Shower Profiles Measured in CMS HCAL and Comparison with Geant4," papers in preparation.

[9] G. Arnison *et al.*, "Hadronic Jet Production at the CERN Proton-Antiproton Collider," Phys. Lett. **B132** 214 (1983).

[10] G. C. Blazey *et al.* "Run II Jet Physics," hep-ex/0005012 v2 (2000).

[11] S.Catani, Y.L.Dokshitzer, M.H.Seymour, B.R.Webber, "Longitudinally Invariant k_{T} Clustering Algorithms for Hadron Hadron Collisions," Nucl. Phys. **B406** (1993) 187.

[12] V. Gavrilov, O. Kodolova, A. Oulianov, and I. Vardanian, "Jet Reconstruction with Pileup Subtraction," CMS Note RN-2003/004 (2003).

[13] CMS TriDAS Project Data Acquisition and High-Level Trigger Technical Design Report CERN/LHCC 2002-26CMS TDR 6.2

[14] S. V. Chekanov, "Jet algorithms: A mini review," hep-ph/0211298.

[15] M.Toennesmann, thesis in preparation.

[16] J. M. Butterworth, J. P. Couchman, B. E. Cox and B. M. Waugh, "KtJet: A C++ implementation of the K(T) clustering algorithm," hep-ph/0210022, Comput. Phys. Commun. **153** (2003) 35.

[17] S. D. Ellis and D. E. Soper, "Successive combination jet algorithm for hadron collisions," hep-ph/9305266, Phys. Rev. D **48** (1993) 3160.

[18] V. D. Elvira, "Jet measurements at DO using a KT algorithm," hep-ex/0209073 (2002).

[19] T. Sjostrand *et al.*, High-energy phisics event generation with PYTHIA 6.1.
Comp.Phys.Com. 135 (2001) pp.238-259.

[20] Object oriented Simulation for CMS Analysis and Reconstruction.
http://cmsdoc.cern.ch/OSCAR/

[21] ORCA user's Guide: http://cmsdoc.cern.ch/orca

[22] CMS JetMET Datasets in DC04 and Post-DC04.
http://cms00.phys.ufl.edu/cms/DC04/PCP/

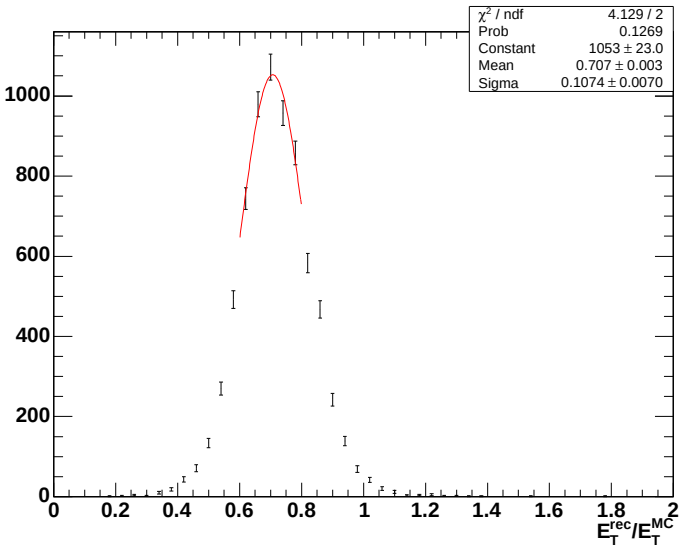

Figure 3: The ratio of reconstructed to generated jet energy for MC jets with E_{T} in the range 105-115 GeV.

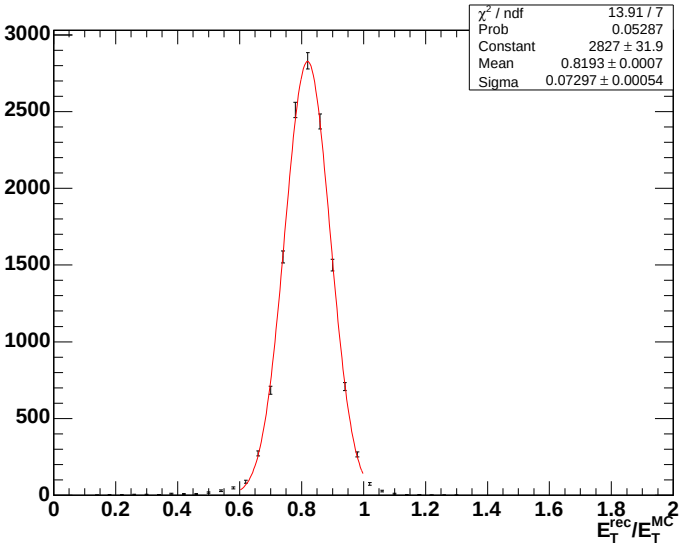

Figure 4: The ratio of reconstructed to generated jet energy for MC jets with E_{T} in the range 300-350 GeV.

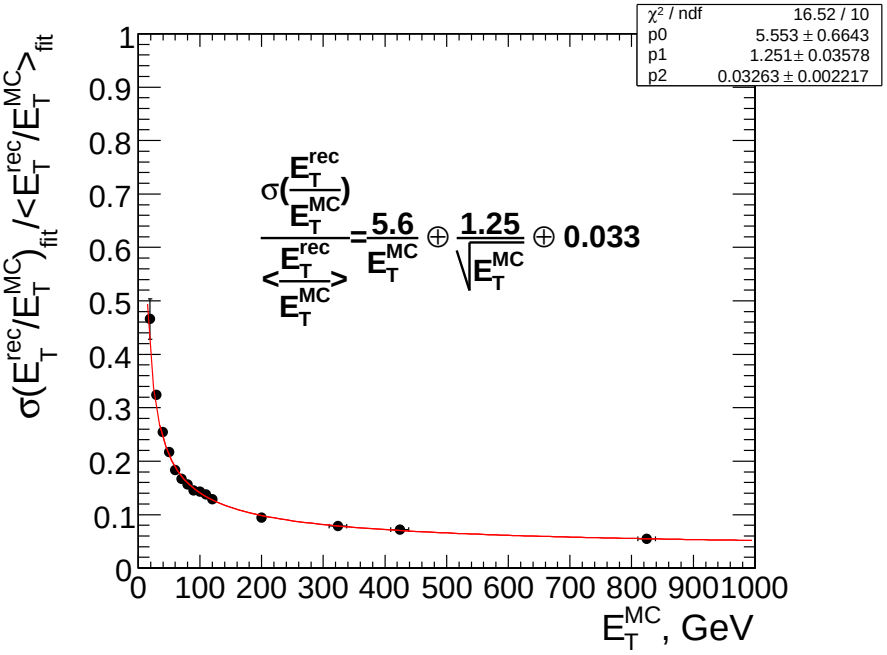

Figure 5: The jet transverse energy resolution as a function of the generated jet transverse energy for barrel jets ($|\eta|$ <1.4). The cuts $E_{\rm T}$ >0.5 GeV and E >0.8 GeV are used. The distance between generated and reconstructed jets is $\Delta R < 0.2$. The Monte Carlo jet calibration is applied.

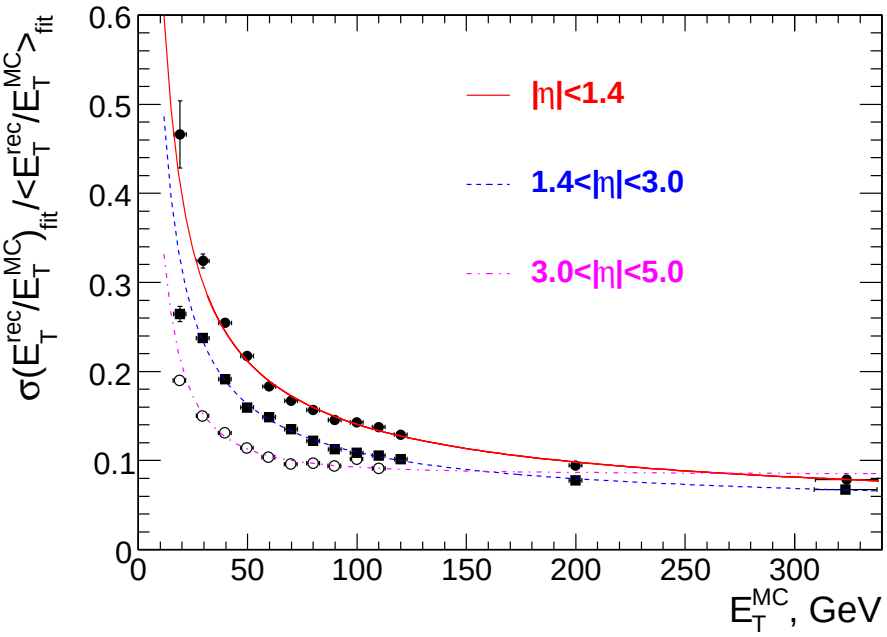

Figure 6: The jet transverse energy resolution as a function of the generated jet transverse energy for barrel jets ($|\eta|$ <1.4), endcap jets (1.4< $|\eta|$ <3.0) and very forward jets (3.0< $|\eta|$ <5.0). The jets are reconstructed with the interative cone $R = 0.5$ algorithm. The cuts $E_{\rm T}$ >0.5 GeV and E >0.8 GeV are used. The distance between generated and reconstructed jets is required to be $\Delta R < 0.2$. The Monte Carlo jet calibration is applied.

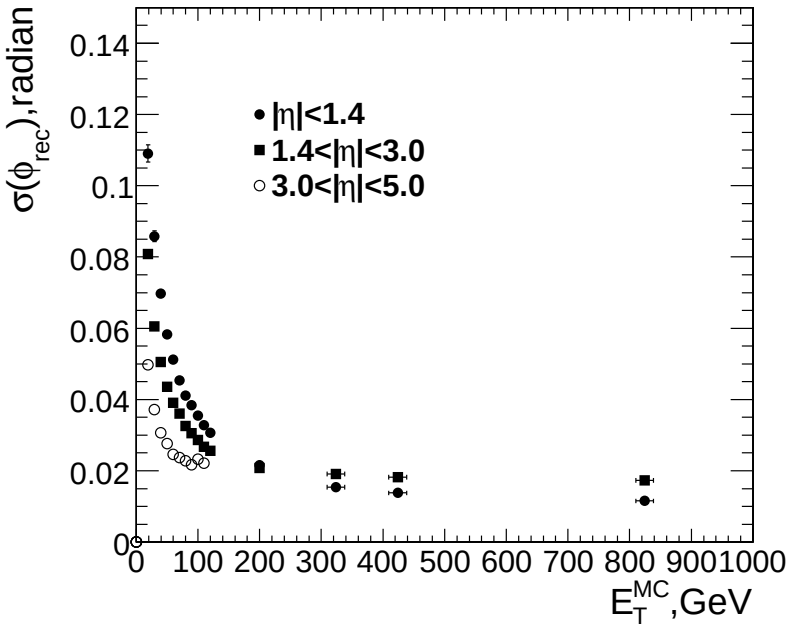

Figure 7: The jet transverse ϕ angular resolution as a function of the generated jet transverse energy for barrel jets ($|\eta|$ <1.4), endcap jets (1.4< $|\eta|$ <3.0) and very forward jets (3.0< $|\eta|$ <5.0). The cuts $E_{\rm T}$ >0.5 GeV and E >0.8 GeV are used. The distance between generated and reconstructed jets is required to be $\Delta R < 0.2$.

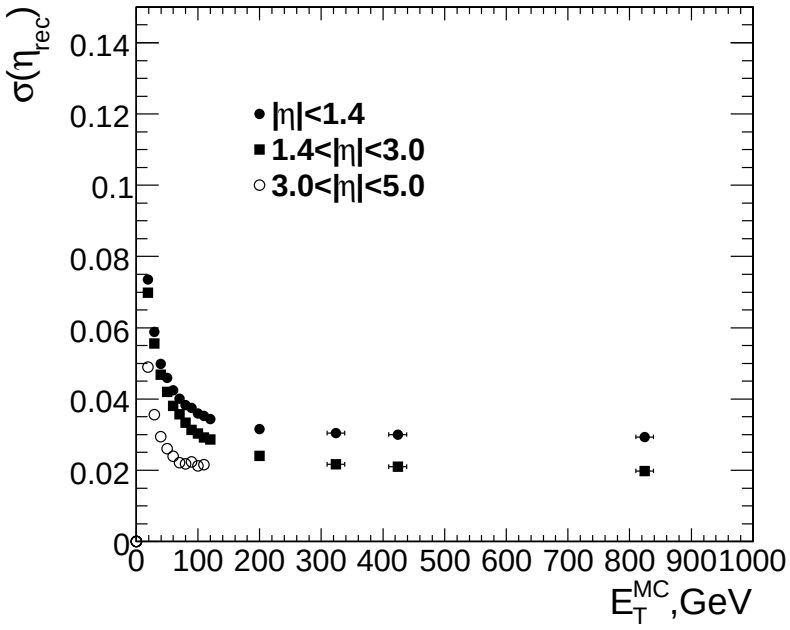

Figure 8: The jet transverse η pseudo-rapidity resolution as a function of the generated jet transverse energy for barrel jets ($|\eta|$ <1.4), endcap jets (1.4< $|\eta|$ <3.0) and very forward jets (3.0< $|\eta|$ <5.0). The cuts $E_{\rm T}$ >0.5 GeV and E >0.8 GeV are used. The distance between generated and reconstructed jets is required to be $\Delta R < 0.2$.